

WL-TR-93-1059

AD-A267 622



DISPLAY OF DYNAMIC, VOLUME GRAPHIC
IMAGES BY HOLOGRAPHIC VOXEL PROJECTION

INITIAL INVESTIGATIONS

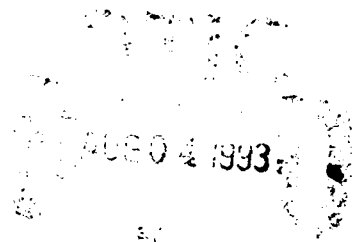


CAPT SHAWN L. KELLY
CAPT CHARLES T. ROBINSON

APRIL 1993

INTERIM REPORT FOR 08/01/89-06/30/91

APPROVED FOR PUBLIC RELEASE; DISTRIBUTION IS UNLIMITED.



AVIONICS DIRECTORATE
WRIGHT LABORATORY
AIR FORCE MATERIEL COMMAND
WRIGHT PATTERSON AFB OH 45433-7409

93-17430



93

8

3

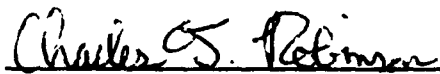
123

NOTICE

When Government drawings, specifications, or other data are used for any purpose other than in connection with a definitely Government-related procurement, the United States Government incurs no responsibility or any obligation whatsoever. The fact that the government may have formulated or in any way supplied the said drawings, specifications, or other data, is not to be regarded by implication, or otherwise in any manner construed, as licensing the holder, or any other person or corporation; or as conveying any rights or permission to manufacture, use, or sell any patented invention that may in any way be related thereto.

This report is releasable to the National Technical Information Service (NTIS). At NTIS, it will be available to the general public, including foreign nations.

This technical report has been reviewed and is approved for publication.



CHARLES T. ROBINSON, CAPT, USAF
Project Engineer



DARREL G. HOPPER, Chief
Cockpit Avionics Office



CHARLES H. KRUEGER, Chief
System Avionics Division

If your address has changed, if you wish to be removed from our mailing list, or if the addressee is no longer employed by your organization please notify WL/AAA, WPAFB, OH 45433-7409 to help us maintain a current mailing list.

Copies of this report should not be returned unless return is required by security considerations, contractual obligations, or notice on a specific document.

REPORT DOCUMENTATION PAGEForm Approved
OMB No. 0704-0188

Public reporting burden for this collection of information is estimated to average 1 hour per response, including the time for reviewing instructions, searching existing data sources, gathering and maintaining the data needed, and completing and reviewing the collection of information. Send comments regarding this burden estimate or any other aspect of this collection of information, including suggestions for reducing this burden, to Washington Headquarters Services, Directorate for Information Operations and Reports, 1215 Jefferson Davis Highway, Suite 1204, Arlington, VA 22202-4302, and to the Office of Management and Budget, Paperwork Reduction Project (0704-0188), Washington, DC 20503.

1. AGENCY USE ONLY (Leave blank)		2. REPORT DATE 29 Apr 93		3. REPORT TYPE AND DATES COVERED Interim, AUG 89 - JUN 91	
4. TITLE AND SUBTITLE Display of Dynamic, Volume Graphic Images by Holographic Voxel Projection/Initial Investigation				5. FUNDING NUMBERS PE 62204 PR 2003 TA 06 WU 64	
6. AUTHOR(S) Capt Shawn L. Kelly Capt Charles T. Robinson					
7. PERFORMING ORGANIZATION NAME(S) AND ADDRESS(ES) Avionics Directorate, Wright Laboratory 2185 Avionics Circle Air Force Materiel Command Wright Patterson AFB OH 45433-7301				8. PERFORMING ORGANIZATION REPORT NUMBER WL-TR-	
9. SPONSORING/MONITORING AGENCY NAME(S) AND ADDRESS(ES) Avionics Directorate, Wright Laboratory 2185 Avionics Circle Air Force Materiel Command Wright Patterson AFB OH 45433-7301				10. SPONSORING/MONITORING AGENCY REPORT NUMBER WL-TR-93-1059	
11. SUPPLEMENTARY NOTES					
12a. DISTRIBUTION/AVAILABILITY STATEMENT Approved for public release; distribution is unlimited.				12b. DISTRIBUTION CODE	
13. ABSTRACT (Maximum 200 words) <p>This document presents in-house research on a Holographic Projector. This device operates by optically guiding the light from each pixel on an internal two-dimensional display to a unique focus in a three-dimensional volume. Properly addressing the 2-D pixel array via conventional computer graphics equipment will, therefore, generate transparent 3-D images which appear to float in space in front of the observer. A detailed mathematical model was created and used to design the Holographic Projector and simulate it's operation. Proof-of-concept experiments were conducted to test the capability of holographic materials to provide the performance predicted by the model. The results of this initial investigation support the continuation of research and development of the Holographic Projector as a special display for applications such as threat warning or directional indication.</p>					
14. SUBJECT TERMS Volume Holography, 3-D Display, Coupled Wave Theory, Holography DuPont Photopolymer				15. NUMBER OF PAGES 51	
				16. PRICE CODE	
17. SECURITY CLASSIFICATION OF REPORT Unclassified	18. SECURITY CLASSIFICATION OF THIS PAGE Unclassified	19. SECURITY CLASSIFICATION OF ABSTRACT Unclassified	20. LIMITATION OF ABSTRACT UL		

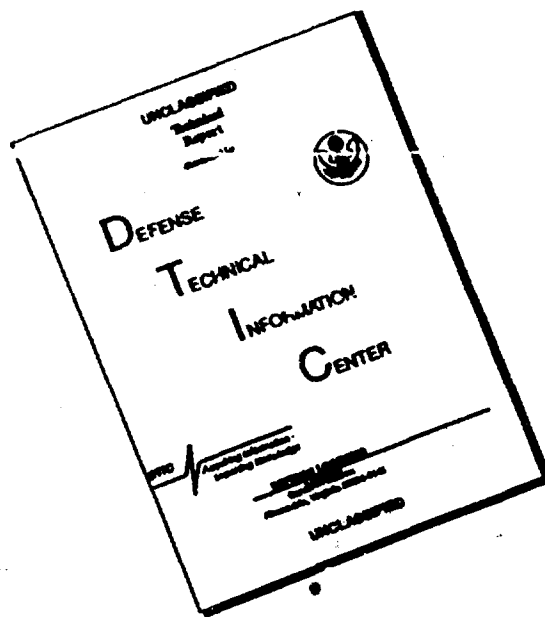
FOREWORD

The purpose of this technical report is to document in-house research accomplished from August 1989 to June 1991 on the Holographic Projector project. Additionally, this document serves as evidence to the claim of invention of the Holographic Projector, Air Force invention number 19,314 (formerly the Volume Graphic Display). Chapter 1 introduces the Holographic Projector as an approach and a device to satisfy commercial and Government needs to display information in three dimensions. Chapter 2 presents the theory behind the fabrication and use of the device. In Chapter 3, the results from Chapter 2 are analyzed and distilled into a practical design of a proof-of-concept Holographic Projector. Chapter 4 describes the fabrication of the device, including materials and equipment used and procedures followed. Chapter 5 offers the results of initial testing. Finally, Chapter 6 gives an analysis of these results, and a conclusion as to the suitability of the Holographic Projector for future research and development.

DTIC QUALITY INSPECTED 3

Accession For	
NTIS GRA&I	<input checked="" type="checkbox"/>
DTIC TAB	<input type="checkbox"/>
Unannounced	<input type="checkbox"/>
Justification	
By _____	
Date _____	
Av _____	
Dis _____	
<div style="font-size: 2em; font-weight: bold; position: absolute; left: 10px; bottom: 10px;">A-1</div>	

DISCLAIMER NOTICE



THIS DOCUMENT IS BEST
QUALITY AVAILABLE. THE COPY
FURNISHED TO DTIC CONTAINED
A SIGNIFICANT NUMBER OF
PAGES WHICH DO NOT
REPRODUCE LEGIBLY.

CONTENTS

Abstract	ii
Foreword	iii
List of Figures	v
1. INTRODUCING THE HOLOGRAPHIC PROJECTOR	1
1.1 Background	1
1.2 The Holographic Projector Approach	1
1.3 The Holographic Projector Program	2
2. MODELLING THE HOLOGRAPHIC PROJECTOR	4
2.1 Introduction	4
2.2 Basics of Phase Volume Holograms	5
2.3 Plane Wave Interference in a Volume Hologram	6
2.4 Plane Wave Diffraction Efficiency Model	7
2.5 Pixel/Voxel Diffraction Efficiency Model	10
2.6 Mapping Efficiency and S/N Formulations	19
2.7 VHS Mapping Algorithm	21
2.8 Holographic Projector Configuration Parameters	21
2.9 Summary of Assumptions and Requirements	22
2.10 Conclusion	23
3. PROOF-OF-CONCEPT POINT DESIGN	24
3.1 Implications of the Holographic Projector Model	24
3.2 Implications of the Mapping Algorithm	26
3.3 The Chosen Proof-of-Concept Architecture	27
4. PROOF-OF-CONCEPT FABRICATION	28
4.1 VHS Configuration and Material	28
4.2 Proof-of-Concept Configuration	28
4.3 Fabrication Equipment Setup	29
4.4 Fabrication Procedures	31
5. EXPERIMENTS AND RESULTS	33
5.1 Experiment 1	33
5.2 Experiment 2	33
5.3 Experiment 3	34
5.4 Experiment 4	34
6. ANALYSIS AND CONCLUSIONS	35
6.1 Analysis	35
6.2 Conclusions	35
REFERENCES	38
App A Mapping Algorithm Computer Code	A-1
App B Plans and Procedures	B-1

LIST OF FIGURES

		pg
1.	Holographic Projector Concept.	2
2.	Reflection vs. Transmission Holograms.	5
3.	Phase Volume Hologram Geometry (2-D View).	7
4.	Geometry for Pixel/Voxel Plane Wave Diffraction Analysis.	11
5.	Plane View of Vector and Ray.	11
6.	Reflection Plane Coordinate System.	14
7.	VHS Segregation into Volume Elements (2-D View).	19
8.	Azimuthal Ray Deviation Geometry.	20
9.	Functional Values of $\sin(\theta_b - \phi)/\sin(2\theta_b)$.	25
10.	Functional Values of $\sin(\theta_b - \phi)/\sin^2(\theta_b)$.	26
11.	Proof-of-Concept Configuration.	29
12.	Proof-of-Concept Fabrication Setup.	30
13.	Diffraction Efficiency vs. Read/Write Beam Angular Deviation for Transmission Holograms.	36
14.	Diffraction Efficiency vs. Read/Write Beam Angular Deviation for Reflection Holograms.	36

1. INTRODUCING THE HOLOGRAPHIC PROJECTOR

This chapter provides the background and motivation for pursuing the development of the Holographic Projector.

1.1. Background.

The electronic display of visual information has historically been constrained to a two-dimensional (2-D) format. This is understandable when one considers that even before the electronic age, a 2-D drawing was the only method of displaying information short of fabricating a model. Of course, many of the subjects we wish to represent actually exist in three dimensions. Consequently, artistic and graphic techniques such as perspective views, hidden line routines, shadowing, hazing and others are required to help us interpret a 2-D rendition as a 3-D scene.

A number of developments have occurred over the last few decades to suggest that we might be able to break free of the 2-D constraint. New approaches to providing a real-time, 3-D capability include variable focus³, volumetric², stereoscopic⁵ and holographic displays⁴. Naturally each of these approaches has its merits and drawbacks¹. Unfortunately, the resulting ratios of these qualities are insufficient to attract significant commercial exploitation.

1.2. The Holographic Projector Approach.

Of the many ways of displaying 3-D images, only those which provide the focus, parallax, perspective and look-around characteristics of a real object scene can provide the full benefit of the third dimension. To date, real-time holography is the only presupposed solution to providing this capability. Such a technique unfortunately requires computational power and real-time media resolution beyond the current state of the art.

The reason holograms require such high resolution is because they store the electromagnetic field characteristics of the many optical wavefronts which comprise an image. With each image, real-time holography requires that these wavefronts must be computed at high resolution and then written to a device to modulate a spatially coherent light beam. All this must also be done at a rate of 30 times per second or greater to avoid image flicker.

The Holographic Projector attempts to take advantage of the capabilities of holography without requiring the exotic devices and computer support involved with holography performed in real-time.

It works by imaging points of light into a volumetric space of fixed volume elements (voxels), just as a conventional monitor places fixed pixels of light on its screen. This implies that the electromagnetic (optical) field characteristics of the wavefronts required to illuminate any voxel are fixed characteristics of the display device. Thus a graphics generator need only drive these stored wavefronts in accordance with the desired intensity of each image voxel. The permanent storage of these high resolution optical field characteristics via volume holography relieves the real-time graphics input device from the necessity of calculating and writing such fields.

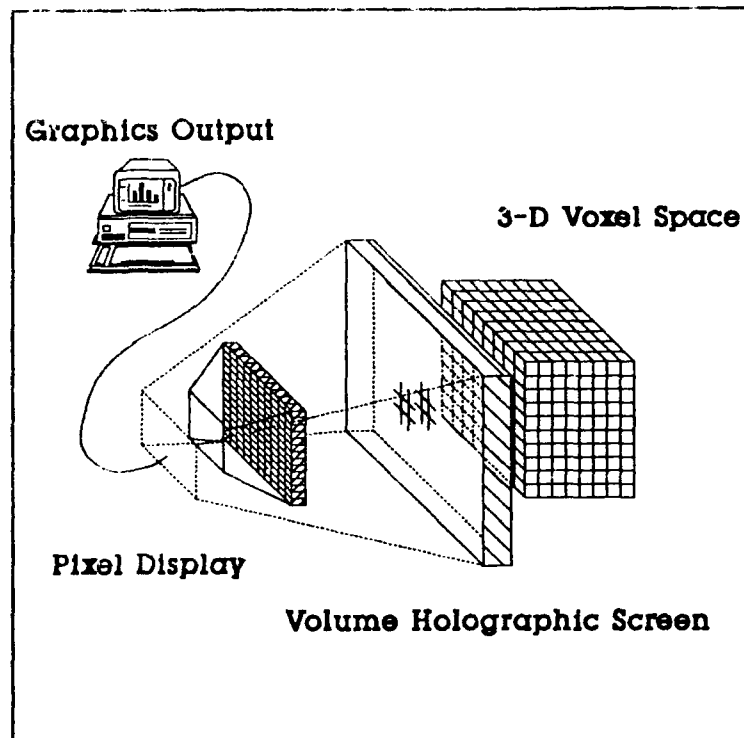


Figure 1. Holographic Projector Concept.

A generalized, conceptual architecture of the Holographic Projector is shown in Figure 1. A light source is projected through a pixel addressable display such as a liquid crystal matrix which is driven by a computer. Associated with each pixel on the display is the mapping of a unique voxel location in the 3-D volume. The optical mapping of all the combinations of pixels and voxels have been permanently stored holographically in a volume hologram called the Volume Holographic Screen (VHS). The VHS thus modulates the phase of the input from each 2-D pixel from the pixel display to create a spherical wave converging to its corresponding voxel. The light passing through the voxel then diverges as it would from an actual point source at that location. The illuminated voxels thus comprise a full 3-D image.

1.3. The Holographic Projector Program.

This program is a task under the WL/XPK inhouse work unit 20030664, "Crew Station Avionics Evaluation." It is funded in response to 3-D display needs in crew station avionics development for future cockpits. Early concept testing will begin within the Crew Systems Integration Laboratory of the Joint Cockpit Office:

WL/XPk. As the first examination of this device and its technology, the scope of this effort has been limited to the use of a minimum of resources required to demonstrate the technology.

This technical report documents work performed in accordance with the following timeline:

Modelling	August, 1989 - February, 1990
Demonstration Design	March, 1990
Equipment Setup	April - November, 1990
Fabrication	November, 1990
Testing	December - March, 1991
Documentation	April - July, 1991

2. MODELLING THE HOLOGRAPHIC PROJECTOR

The purpose of this analysis is to first, provide an understanding of the two-dimensional (2-D) to three-dimensional (3-D) mapping issues associated with the Holographic Projector and second, provide a first-order physical model of the Holographic Projector which is sufficient to simulate the performance of various component configurations and mapping strategies.

2.1. Introduction.

In summary, the Holographic Projector operates by optically mapping each pixel on a 2-D input plane to a unique, floating, volume element (voxel) in a 3-D image space. This capability is provided by the combination of a spatially-controllable grid of independent point-sources of light (the pixels) and a specially created Volume Holographic Screen (VHS). The light from each point source is diffracted by the VHS into a spherical wave which converges on its corresponding voxel. This light continues to propagate while diverging from each voxel toward the viewer. The viewer's eyes then focus the divergent light and interpret this input as that emitted from point source located at the corresponding voxel position.

It is apparent that the technically significant component of the Holographic Projector is the Volume Holographic Screen. Accordingly, the properties of volume holograms yield several issues which must be addressed in the development of this component and the resultant Holographic Projector configuration. The most important issue is that of diffractive crosstalk. A volume hologram is essentially a 3-D diffraction grating. This holographic grating is formed by the 3-D interference pattern formed by the light from each coherent pixel/voxel combination. Ideally, each pixel point source will be diffracted only to a single voxel. Unfortunately, diffraction gratings are generally not 100 percent efficient. Quantitatively, diffraction efficiency is the amount of energy of the diffracted beam divided by that of the input beam. If the VHS is improperly configured, the conditions which govern diffraction efficiency will provide an opportunity for the light from one pixel to diffract into more than one voxel. Essentially, our objective must be to manipulate these conditions via a selected mapping scheme such that diffraction efficiency is maximized for each correct pixel/voxel combination, while minimized for all other pixel light sources trying to propagate to that same voxel.

The second issue resulting from the properties of volume holograms concerns deciding what kind of volume hologram is best

and in what configuration. Since high overall diffraction efficiency is important, phase holograms are preferable over amplitude holograms. However, the orientation of the pixel plane, VHS and image space during formation and in use cannot be determined until the mapping analysis has been completed.

With these issues in mind, the first step in analyzing the Holographic Projector is to develop a generic model for a phase volume hologram which relates diffraction efficiencies to pixel/voxel geometries and hologram properties. Throughout this analysis, it will be assumed that the VHS will perform as an ideal phase holographic medium wherein the index variations in the material represent a linear superposition of the intensities created by interfering each coherent pixel and voxel source combination.

2.2. Basics of Phase Volume Holograms.

There are two general types of phase volume holograms to be considered - transmission and reflection. In either case, there is always a reference beam and an object beam involved in the hologram's formation. The effect of storing the interference of these beams is to set up reflection surfaces within the medium. Such surfaces are always parallel to the bisector of the angle formed by the intersection of the two rays. The characteristics which

distinguish the two types of holograms are illustrated in Figure 2. If both "writing" beams strike the same side of the holographic medium, then reflection surfaces are created which will transmit light through the medium when illuminated by the same reference beam - yielding a transmission hologram. If the writing beams are on opposite sides of the medium, then the created reflection surfaces will effectively reflect light from the medium when illuminated by the same reference beam - yielding a reflection

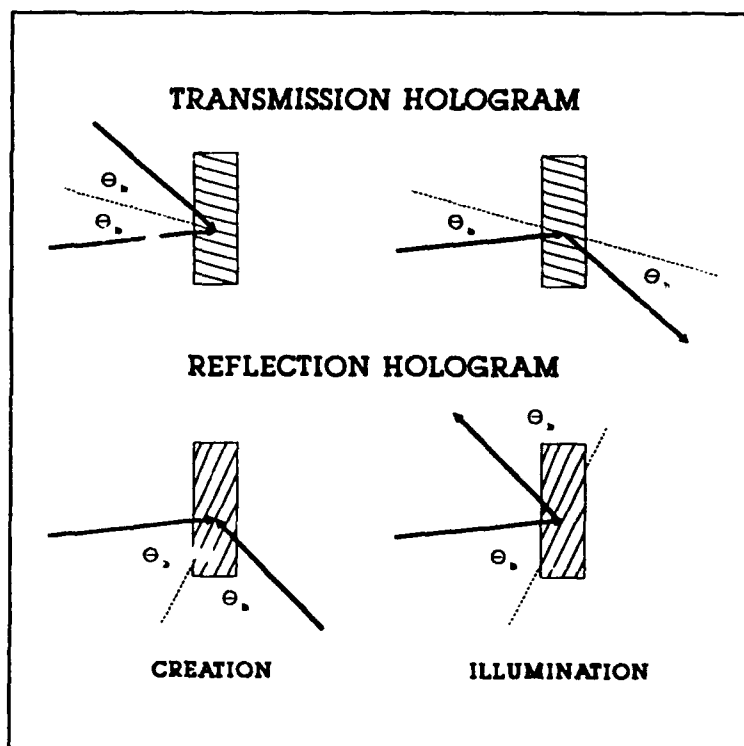


Figure 2. Reflection vs. Transmission Holograms.

hologram. In either case, the resultant image beam is generated by the complicated structure of the reflection surfaces.

An important quantity shown in Figure 3 is the Bragg angle (θ_b). While simply illustrated in this case, the Bragg angle plays a major role in the much more complicated analysis to follow. It is important to remember that this quantity is a fixed property of the hologram once it is formed.

2.3. Plane Wave Interference in a Volume Hologram.

The Volume Holographic Screen is an optical device in which variations in optical path length (most likely through index variations) are proportional to the superposition of intensities of each pixel/voxel interference pattern created during the VHS formation. Each of these interference patterns, or fringe patterns, will be the coherent vector addition of the spherical waves coming from the pixel and voxel locations. The effect of these interference patterns in a generic volume hologram is to create reflection surfaces within the holographic medium. Now, if any area of the VHS is examined in small enough detail, the spherical waves can be approximated as plane waves. This idea allows us to analyze the entire VHS as the storage of plane wave interference patterns which as a whole act as spherical wave interference patterns.

When two plane waves coherently interfere, the resultant intensity maxima, measured in the plane formed by the intersecting propagation vectors, form a periodic lattice much like that of a crystal lattice of atomic centers (normal to this intersection, the intensity distribution is constant). This analogy justifies the wide-spread use of the Bragg diffraction model to describe volume hologram effects. The model explains that the lattice is formed of reflection planes which effectively reflect and refract radiation through diffraction. The influence of these effects is generally dependent on the spacing of the reflection planes. The relation which brings these parameters together is the Bragg equation, $2d\sin(\theta_b) = \lambda$, where d is the spacing between the planes, θ_b is the Bragg angle and λ is the wavelength (all in the material).

It is very important that two applications of the Bragg equation are seen in holography. First, when the hologram is formed, this equation will reveal the separation of the created planes of the lattice. Now the parameters of the Bragg equation are all known and the hologram has a fixed structure. The second application then involves using this equation with the appropriate parameters to model the behavior of light incident on the hologram. This behavior is now characterized by Bragg diffraction. This phenomenon provides that deviations in the incident light which do not satisfy the Bragg equation will be strongly attenuated. On the

other hand, incident light which does satisfy the Bragg equation will be reflected from the planes as shown in Figure 2 (that is, the angle of incidence equals the angle of reflection from the plane). These concepts of creating lattices and analyzing Bragg diffraction are central to the much more robust theory to follow.

2.4. Plane Wave Diffraction Efficiency Model.

The most pervasive model of volume holograms is given by the "coupled-wave theory" originally described by Herwig Kogelnik in 1969⁶. While the following discussions will be given in the context of the VHS formation, the resultant formulations are entirely based on his work with assistance from the book Optical Holography, by Collier, et al in 1971⁷. In fact, the derivation of these models will be kept to a minimum to avoid duplicity.

2.4.1. Geometry.

Figure 3 illustrates the basic geometry involved in developing the models for phase volume holograms. The index outside of the material is assumed to be identical to that inside. This assumption will be corrected further in the development. The given geometry is generic to both types of holograms described and serves as a condensed version of Kogelnik's development. As such, only certain parameters which appear in this paper are illustrated.

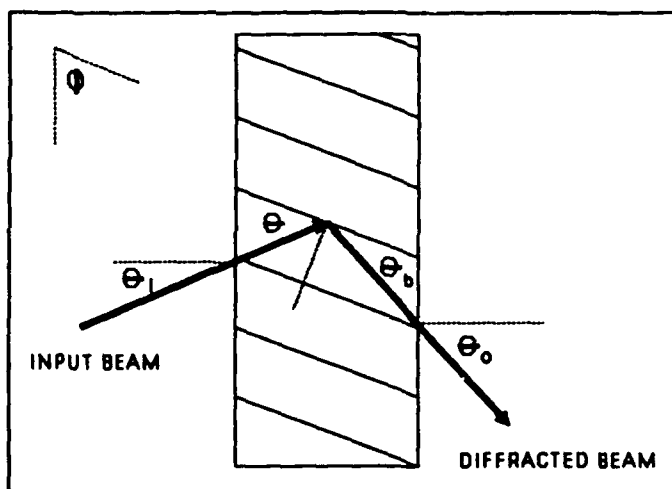


Figure 3. Phase Volume Hologram Geometry (2-D View).

2.4.2. Symbols and Definitions.

The following definitions will be used throughout the discussion.

- λ_0 The wavelength of light in air.
- n_0 The average index of refraction of the VHS.

n_a	The index of refraction of air.
n_1	The maximum amplitude of the periodic index grating formed by the write beam interference.
T	The thickness of the VHS.
θ_b	The Bragg angle of the formed grating, measured as the angle between the reflection plane and the diffracted beam.
θ	The incident angle of an arbitrary read beam, measured as the angle between the beam and the reflection plane.
θ_i	The incidence angle of the writing beam, measured as the angle between the ray and the normal to the VHS face.
θ_o	The incidence angle of the exiting beam, measured as the angle between the ray and the normal to the VHS face.
δ	The angular deviation of an incident ray from the Bragg angle, measured in radians as $\theta - \theta_b$.
Δ	The difference in wavelength between the read beam and that of the writing beam which formed the hologram.
ϕ	The slant angle which is measured as the angle between the reflection plane and the face of the VHS.
η	Diffraction efficiency, measured as the energy in the diffracted beam over that of the incident beam.

2.4.3. Initial Assumptions and Qualification of Theory.

The coupled wave theory primarily assumes that the hologram is thick enough that illuminating configuration deviations from the Bragg equation are quickly attenuated and that diffraction efficiencies are high. In general, although other assumptions exist, the theory has been experimentally validated for the types of holograms we will be making.⁸ Of course, we continue to assume that the formation of any pixel/voxel hologram is entirely unaffected by that of any other. We also assume that the holograms are lossless and that internal reflections are negligible. The next section describes a basic diffraction formulation for writing beams polarized in the plane of incidence. Further in the development, these equations will be generalized for a more realistic scenario.

2.4.4. Diffraction Efficiency Formulations in Volume Holograms.

The following equations assume that the index outside the hologram is identical to the average index inside the material. The diffraction efficiencies essentially yield the sensitivity of a preformed hologram to not only the characteristics of that formation, but also to deviations in the wavelength and the

incidence angle of illuminating light.

For transmission holograms, the diffraction efficiency is

$$\eta_t = \frac{\sin^2(\sqrt{\alpha^2 + \beta^2})}{(1 + \frac{\alpha^2}{\beta^2})} \quad (1)$$

and for reflection holograms, the diffraction efficiency is¹

$$\eta_r = \frac{1}{\frac{\alpha^2}{\beta^2} + (1 - \frac{\alpha^2}{\beta^2}) \coth^2(\sqrt{\beta^2 - \alpha^2})} \quad (2)$$

where

$$\alpha = \frac{\pi T n_o}{C_s \lambda_a} \sin(2\Theta_b) \left(\delta + \frac{\Delta \tan(\Theta_b)}{\lambda_a} \right) \quad (3)$$

$$\beta = \frac{i\pi n_1 T}{\lambda_a \sqrt{C_r C_s}} \quad (4)$$

$$C_r = \cos(\Theta_i) \quad \text{and} \quad C_s = \cos(\Theta_o) \quad (5)$$

¹. These equations are extracted from Kogelnik (denoted as K-#) and Collier (denoted as C-#) as follows. Equation (1) comes from K-43; (2) from K-57 (converted into a coth form); (3) from C-9.75 and C-9.105a as modified to show responses to δ and Δ by Collier, page 249. This equation has also been generalized for arbitrary slant angle ϕ (the slant angle is embedded in Θ_i and Θ_o). Equation (4) comes from C-9.76 and C-9.105b, again generalized for arbitrary slant; and Equation (5) comes from C-9.61 and the geometry described in Fig. 9.3 in Collier. For background, although both referenced presentations are similar, Collier sacrifices the treatment of slanted gratings for a more concise discussion. The i in Equation (4) only applies to reflection holograms.

2.4.5. Condition for Plane-Wave Diffraction Efficiency Model.

The equations developed in this section assume that deviations from the Bragg condition, as well as other diffraction orders which satisfy this condition, are strongly attenuated due to the thickness of the hologram. Although the validity of this assumption is not directly presented by the two references, they claim that sufficient analysis has been performed by Klein to conclude that the plane-wave diffraction efficiency model given above is reasonable under the condition:⁹

$$\frac{8\pi\sin^2(\theta_b) n_o T}{\lambda_a} > 10 \quad (6)$$

Fortunately, this condition justifies the use of the previous equations in all cases except those where the bragg angle is less than a calculated general limit of roughly four degrees.

2.5. Pixel/Voxel Diffraction Efficiency Model.

To be useful, the diffraction efficiency equations (Equations (1) and (2)) must be recast in terms of the Holographic Projector geometry as a function of the form $\eta(a,b,c;f,g,h;f_q,g_q,h_q;m,n)$. This function is a challenging equation to derive because of its dependence on the three-dimensionality of the geometry and the interaction of three points. The function can be described as: ~~what is~~ the diffraction efficiency in the direction of a voxel point at (a,b,c) ; given a pixel point at (f,g,h) ; going through the VHS at point (m,n) where the grating at (m,n) was formed by the pixel at (f_q,g_q,h_q) and the voxel at (a,b,c) . See Figure 4. Inherent in the function is the knowledge of the examined pixel/voxel combination $(a,b,c;f_q,g_q,h_q)$ used to form the grating by virtue of the Bragg angle and the slant angle created by their interference.

The calculation of η requires the values of θ_b , θ_1 , θ_0 and δ . A convenient approach to obtain these values is to derive a new orthogonal coordinate system based on the reflection plane geometry resultant from the grating formation. The derivation begins with a vector formulation of the rays arriving at point P (representing the center of the VHS thickness at point $(x=m,y=n)$) in the medium from the voxel and pixel points described in the desired η function. The geometry, shown in Figure 4, is shown for the formation of a reflection hologram, although the derivations are

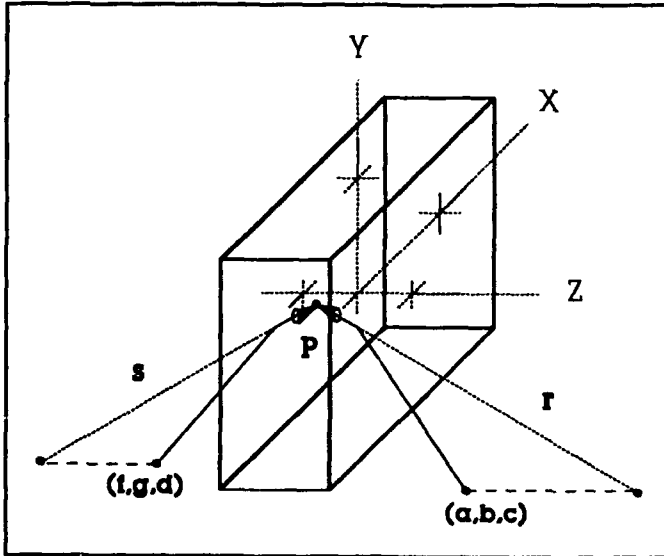


Figure 4. Geometry for Pixel/Voxel Plane Wave Diffraction Analysis.

equally applicable to the transmissive case.

2.5.1. VHS Vector Ray Formulation.

We define \mathbf{r} as the vector (all vectors are in bold face) from a voxel point at $(x=a, y=b)$ to P, but collinear with that portion of the light ray from (a,b,c) to P which is refracted by the change in index of the VHS. Since the x and y components of \mathbf{r} and the ray from the voxel are identical, we need only determine the z component

(r_z) of \mathbf{r} to completely determine the vector's form. Figure 5 shows a useful view of the plane which contains both the voxel ray and the vector. Some additional symbols are shown to aid in the analysis.

Simple trigonometry reveals that

$$\sin(\Theta_2) = \frac{v}{u} \quad (7)$$

$$\sin(\Theta_1) = \frac{w}{q} \quad (8)$$

Now, by Snell's law,

$$n_a \sin(\Theta_1) = n_o \sin(\Theta_2) \quad (9)$$

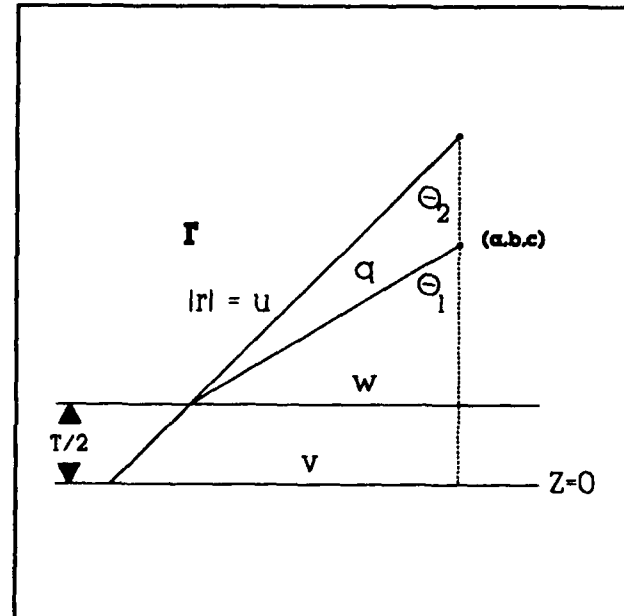


Figure 5. Plane View of Vector and Ray.

Thus

$$\frac{n_a w}{Q} = \frac{n_o v}{u} \quad (10)$$

Also,

$$r_z^2 + v^2 = u^2 \quad (11)$$

and

$$(c - \frac{T}{2})^2 + w^2 = Q^2 \quad (12)$$

We now make the simplifying assumption that the thickness of the VHS is small enough that $w \sim v$ and $(c-T/2) \sim c$. The last three equations can then be combined to yield

$$r_z = \pm \left(\frac{n_o}{n_a} \right) \sqrt{c^2 + v^2 \left(1 - \frac{n_a^2}{n_o^2} \right)} \quad (13)$$

where the value of v^2 is given by

$$v^2 = (m-a)^2 + (n-b)^2 \quad (14)$$

and the choice of + or - is opposite the sign of c .

The value of r_z can now be used to generate the form of the vector \mathbf{r} as

$$\mathbf{r} = (m-a)\mathbf{i} + (n-b)\mathbf{j} + r_z\mathbf{k} \quad (15)$$

where \mathbf{i} , \mathbf{j} and \mathbf{k} are the unit vectors of the Holographic Projector coordinate system.

This derivation can be applied to any arbitrary ray entering or exiting the VHS. Thus the ray to point P from the pixel location is accordingly given by

$$\mathbf{s} = (m-f)\mathbf{i} + (n-g)\mathbf{j} + s_z\mathbf{k} \quad (16)$$

2.5.2. Alternative Coordinate System Formation.

We now use the vectors \mathbf{r} and \mathbf{s} (which represent the propagation of the writing plane waves in the medium) with our knowledge of how the diffraction planes are formed to develop a new coordinate system centered on the general point P. Since only the directions of these vectors are important, we first convert them into unit vectors such that

$$\underline{\mathbf{r}} = \frac{r_x\mathbf{i} + r_y\mathbf{j} + r_z\mathbf{k}}{\sqrt{r_x^2 + r_y^2 + r_z^2}} \quad (17)$$

and a similar expression for $\underline{\mathbf{s}}$ (all underlined vectors are unit vectors). The coordinate system of interest is shown in Figure 6. The vectors $\underline{\mathbf{r}}$ and $\underline{\mathbf{s}}$ form a plane (not the reflection plane) which contains the new orthogonal unit vectors \mathbf{j}' and \mathbf{k}' , with \mathbf{j}' defined as the anti-bisector of the directions of $\underline{\mathbf{r}}$ and $\underline{\mathbf{s}}$. \mathbf{i}' then completes the orthogonal system as the direction perpendicular to $\underline{\mathbf{r}}$ and $\underline{\mathbf{s}}$.

Since $\underline{\mathbf{r}}$ and $\underline{\mathbf{s}}$ are normalized, the unit vector in the direction of their bisection can easily be determined by vector addition. Thus

$$\mathbf{j}' = \frac{-(\underline{\mathbf{r}} + \underline{\mathbf{s}})}{|\underline{\mathbf{r}} + \underline{\mathbf{s}}|} \quad (18)$$

i' can be determined from the cross product of the two normalized vectors as given by

$$i' = s \times r \quad (19)$$

k' is now similarly found by the cross product of Equations (18) and (19).

$$k' = i' \times j' \quad (20)$$

2.5.3. Geometric Formulation of η .

Thus far we have developed a reference coordinate system for the reflection plane (that formed by i' and j') formed by the voxel and pixel position given in the η function. It now becomes very simple to determine the values of θ_b , θ_1 , θ_0 and δ . From Figure 6 we see that θ_b is simply the angle between the vectors r and j' . This value is therefore found by a dot product of these two vectors such that

$$\theta_b = \arccos(-r \cdot j') \quad (21)$$

The deviation from the Bragg angle can be found by a three step process. The new pixel ray which is being analyzed is first converted into a vector p within the VHS just as s was converted. The angle of incidence, θ , of p with the reflection plane is then determined by a dot product:

$$\theta = \arccos(-p \cdot k') \quad (22)$$

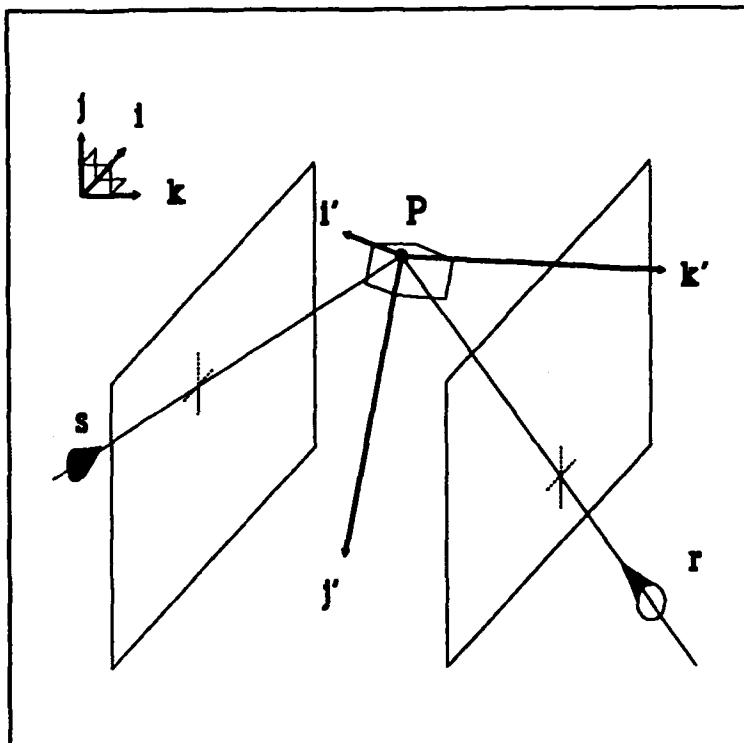


Figure 6. Reflection Plane Coordinate System.

The deviation of this ray from the Bragg angle is therefore given by

$$\delta = \theta - \theta_b \quad (23)$$

Finally, the VHS face incident angles are given by

$$\theta_i = \arccos(\mathbf{r}_z) \quad (24)$$

$$\theta_o = \arccos(\mathbf{g}_z) \quad (25)$$

These formulations can now be used to fully determine the diffraction efficiency, η , given only the parameters in its functional form, $(a,b,c;m,n;f,g,h;f_q,g_q,h_q)$, and certain constants of the Holographic Projector configuration.

2.5.4. Extension to Arbitrary Polarization.

Thus far the diffraction efficiency formulas have assumed that the polarization of the writing vectors has been such that both electric field vectors are collinear. In fact, the general case will not yield this optimum condition. Kogelnik provides the necessary extension to general polarizations in his appendix. The result is an understandable modulation of the coupling by the dot product of the two electric field vectors. The additional assumptions involved are included in Section 2.9. The modulation is applied by including the resultant dot product as a multiplicative term in Equation (4).

The electric field vectors of interest are perpendicular to the vectors \mathbf{r} and \mathbf{g} . We now require the polarization of both rays to be parallel to the y-z (vertical) plane for simplicity. In this case, both electric field vectors must also be perpendicular to the x axis. Finally, we restate the assumption that the amplitude of all the rays are assumed to be identical. Thus the electric field vectors of both writing rays are essentially unit vectors of those fields.

The above information is sufficient to determine the coupling modulation by simple vector analysis. Since the electric field

unit vectors \underline{E}_r and \underline{E}_s are perpendicular to \underline{i} and to their respective rays, we can write

$$\underline{E}_r = \underline{r} \times \underline{i} \quad (26)$$

$$\underline{E}_s = \underline{s} \times \underline{i} \quad (27)$$

We now define the coupling modulation as M , and determine its value as

$$M = \underline{E}_r \cdot \underline{E}_s = (\underline{r} \times \underline{i}) \cdot (\underline{s} \times \underline{i}) \quad (28)$$

$$= (\underline{r} \cdot \underline{s}) (\underline{i} \cdot \underline{i}) - (\underline{r} \cdot \underline{i}) (\underline{s} \cdot \underline{i}) \quad (29)$$

$$= \underline{r} \cdot \underline{s} - \underline{r}_x \underline{s}_x \quad (30)$$

$$M = \underline{r}_y \underline{s}_y + \underline{r}_z \underline{s}_z \quad (31)$$

2.5.5. Summary of Plane Wave Diffraction Efficiency Model.

The developments of Sections 2.4 and 2.5 are consolidated in the following recipe for determining the plane wave diffraction efficiency function. In addition, the equations are presented in order of available component formulas to facilitate the computer implementation to follow. Thus η , as a function of a , b , c , f , g , h , f_q , g_q , h_q , m , n and other scenario parameters from Section 2.4.2 is determined by completing the following steps. Note that since we are seeking angular selectivity for the mapping scheme, the wavelength dependence has been removed from Equation (45).

$$r_z = \pm \left(\frac{n_o}{n_a} \right) \sqrt{c^2 + [(m-a)^2 + (n-b)^2] \left[1 - \frac{n_a^2}{n_o^2} \right]} \quad (32)$$

$$s_z = \pm \left(\frac{n_o}{n_a} \right) \sqrt{h_q^2 + [(m-f_q)^2 + (n-g_q)^2] \left[1 - \frac{n_a^2}{n_o^2} \right]} \quad (33)$$

$$p_z = \pm \left(\frac{n_o}{n_a} \right) \sqrt{h^2 + [(m-f)^2 + (n-g)^2] \left[1 - \frac{n_a^2}{n_o^2} \right]} \quad (34)$$

$$\mathbf{r} = \frac{(m-a)\mathbf{i} + (n-b)\mathbf{j} + (r_z)\mathbf{k}}{\sqrt{(m-a)^2 + (n-b)^2 + r_z^2}} \quad (35)$$

$$\mathbf{s} = \frac{(m-f_q)\mathbf{i} + (n-g_q)\mathbf{j} + (s_z)\mathbf{k}}{\sqrt{(m-f_q)^2 + (n-g_q)^2 + s_z^2}} \quad (36)$$

$$\mathbf{p} = \frac{(m-f)\mathbf{i} + (n-g)\mathbf{j} + (p_z)\mathbf{k}}{\sqrt{(m-f)^2 + (n-g)^2 + p_z^2}} \quad (37)$$

$$\mathbf{i}' = \mathbf{s} \times \mathbf{r} \quad (38)$$

$$\mathbf{j}' = \frac{-(\mathbf{r} + \mathbf{s})}{|\mathbf{r} + \mathbf{s}|} \quad (39)$$

$$\mathbf{k}' = \mathbf{i}' \times \mathbf{j}' \quad (40)$$

$$\Theta = \arccos(-\mathbf{p} \cdot \mathbf{k}') \quad (41)$$

$$\Theta_b = \arccos(-\mathbf{r} \cdot \mathbf{j}') \quad (42)$$

$$\delta = \Theta - \Theta_b \quad (43)$$

$$\beta^2 = \left[\frac{\pm 1}{\mathbf{r}_z \mathbf{s}_z} \right] \left[\frac{\pi n_1 T (\mathbf{r}_y \mathbf{s}_y + \mathbf{r}_z \mathbf{s}_z)}{\lambda_a} \right]^2 \quad (44)$$

$$\alpha^2 = \left[\frac{\delta \pi T n_o \sin(2\Theta_b)}{\mathbf{s}_z \lambda_a} \right]^2 \quad (45)$$

$$\eta_t = \frac{\sin^2(\sqrt{\alpha^2 + \beta^2})}{(1 + \frac{\alpha^2}{\beta^2})} \quad (46)$$

$$\eta_r = \frac{1}{\frac{\alpha^2}{\beta^2} + (1 - \frac{\alpha^2}{\beta^2}) \coth^2(\sqrt{\beta^2 - \alpha^2})} \quad (47)$$

2.6. Mapping Efficiency and S/N Formulations.

The last section concluded with formulas for diffraction efficiencies given plane wave interference. To treat the spherical waves associated with pixels and voxels, we consider the VHS face as the equivalent of $M \times N$ equal volume elements. We assume that if these elements are small enough, then the effects of interference and diffraction can be adequately explained by plane wave interference. A 2-D illustration of this scenario is shown in Figure 7.

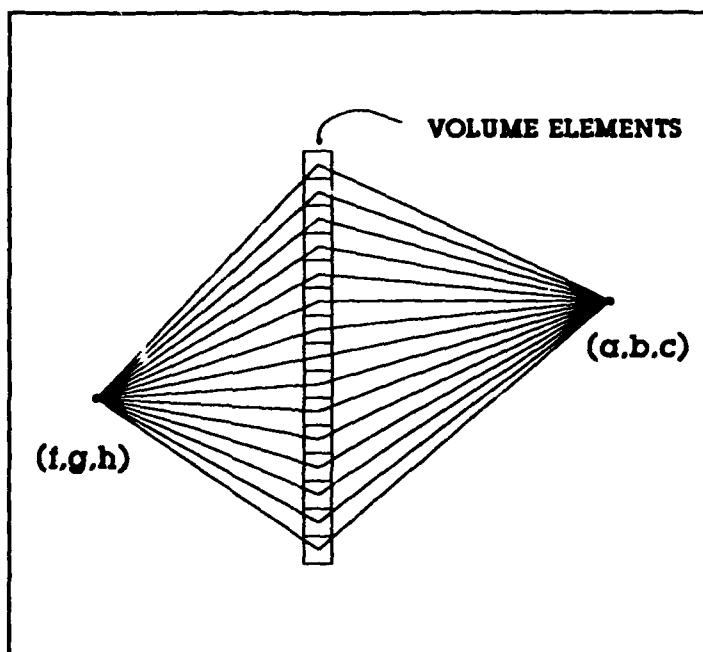


Figure 7. VHS Segregation into Volume Elements (2-D View).

We now define the term mapping strength (MS) as the sum of the diffracted intensities from a pixel location, through each volume element of the VHS, and to a particular voxel location. Mathematically, this value is defined as

$$MS(a, b, c; f, g; f_q, g_q) = \sum_{m=1}^M \sum_{n=1}^N \eta(a, b, c; m, n; f, g; f_q, g_q) \quad (48)$$

where m and n are coordinate indices of the volume element (the function converts the indices to actual locations). Note that it is assumed that square law and interface reductions in intensity are negligible.

The final definition we will make is that of the signal-to-noise ratio (S/N). Qualitatively, this value is the MS of a given writing pixel/voxel combination divided by the aggregate image energy of all other pixels propagated through the VHS resultant

from that combination. This takes on the mathematical form of

$$S/N = \frac{MS(a, b, c; f=f_q, g=g_q; f_q, g_q)}{\sum_{f=1}^F \sum_{g=1}^G \sum_{m=1}^M \sum_{n=1}^N \eta(a, b, c; m, n; f, g; f_q, g_q) Q(a, b, c; m, n; f, g)} \quad (49)$$

where f and g are coordinate indices of all the pixel locations except for that of f_q, g_q . The inner sum reflects the energy which is diffracted by the VHS from a given pixel of index (f, g) . The outer sum simply adds this energy for all pixels. The function Q is an estimate of the attenuation of radiation which arrives at a volume element which has an azimuth other than that of the incident ray which created the grating. The scenario is illustrated in Figure 8, where ray A represents an input ray with the same azimuth as the original writing ray, and ray B has an azimuth other than ray A of an azimuthal separation angle of σ . This attenuation is assumed to occur because ray B is likely to pass through nonsupportive Bragg conditions as it propagates through other regions of the VHS.

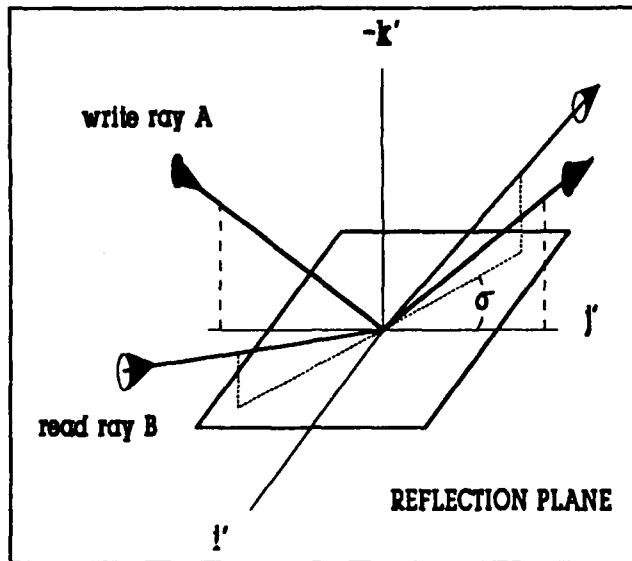


Figure 8. Azimuthal Ray Deviation Geometry.

Although a detailed analysis may be necessary, it will be assumed for this model that this attenuation is in the form $Q = \cos^2(\sigma)$, where the value of σ can be simply found as the angle between the projections of rays A and B onto the reflection plane. Since such a projection for ray A defines the direction of j' (see Fig. 8), the value of Q can be derived as

$$Q = \frac{1}{1 + \left[\frac{B \cdot j'}{B \cdot i'} \right]^2} \quad (50)$$

We can now specify our goal quantitatively as the determination of a pixel/voxel mapping strategy which maximizes the aggregate signal-to-noise ratio for the entire Holographic Projector.

2.7. VHS Mapping Algorithm.

The maximization of the aggregate Holographic Projector S/N is a highly computer intensive task. As a first order alternative, each voxel will be **sequentially** analyzed to determine its best pixel counterpart. If the chosen pixel has already been assigned to a previous voxel, the next best available pixel will be chosen. The algorithm to generate this mapping is shown to the right.

```

For all voxels =>
  o Set Temporary S/N (TSN) = 0
  o For all unassigned pixels =>
    o Find S/N
    o If (S/N>TSN) =>
      o De-assign any
        previous
          assignments for this
            voxel
      o Assign current pixel
        to
          current voxel
      o Set TSN = S/N
    <==
  <==
<==

```

VHS Mapping Algorithm

2.8. Holographic Projector Configuration Parameters.

The most desirable configuration of the Holographic Projector components is ultimately determined by the best aggregate S/N which can be obtained within a given parameter space. The important geometry parameters are as follows:

dv	The distance between voxels in x, y and z.
dp	The distance between pixels in f and g.
Vx, Vy, Vz	The location of the center of the voxel volume.
Px, Py, Pz	The location of the center of the pixel array.
θ_v, θ_p	The angle of the pixel and voxel arrays from the x axis, where a positive angle is measured clockwise, looking parallel to the direction of the y axis onto the x-z plane (ref. Fig. 4).
ϕ_v, ϕ_p	The angle of the pixel and voxel arrays from the y axis, where a positive angle is measured clockwise, looking parallel to the direction of the x axis onto the y-z plane (ref. Fig. 4).

These parameters, combined with λ_a , n_o , n_1 and T (n_a is assumed to be unity), comprise the full parameter space which must be examined. Thus, the next chapter will apply variations in these sixteen parameters in an analysis of the Holographic Projector's performance. The trends which result will then be examined to choose a suitable experimental prototype configuration.

2.9. Summary of Assumptions and Requirements.

A large number of assumptions have been made in this chapter to provide a relatively simplified model of the physics involved with the Holographic Projector. This section consolidates those which have been made and presents others which are necessary to qualify such a model.

1. The device used as a pixel array contains pixels which are approximated by points.

2. The non-uniform loss of energy across the surface of the VHS due to changing transmission coefficients is assumed to be negligible.

3. The VHS material is assumed to be non-polarization sensitive and also void of any polarizing properties.

4. The VHS is assumed to be reasonably approximated by a number of volume elements wherein the diffraction can be attributed to a structure of diffraction planes which vary sinusoidally in refractive index along the normal to those planes.

5. The thickness of the VHS is assumed to be sufficiently less than the distance from the VHS surface to any voxel or pixel. This assumption supports the assumption that the diffraction plane structure in any VHS volume element can be characterized by a geometric approximation (ref. Section 2.5.1).

6. The VHS can store as many sinusoidal holograms of index amplitude n_1 as there are voxels, where the storage of one such hologram does not affect any previously written holograms.

7. The VHS material is assumed to be capable of storing sinusoidal gratings of all the spatial frequencies involved in any given pixel/voxel combination.

8. The hologram is a thick hologram in that gross deviations from Bragg conditions are assumed to be attenuated. This assumption requires compliance with Equation (6).

9. Internal reflections are assumed to be negligible in either the writing or reading stage.

10. The VHS is a lossless, homogeneous recording material with a permeability of 1 and a conductivity of 0.

11. Square law losses in intensity due to path differences of pixel and voxel rays are assumed to be negligible.

12. The amplitude of any sinusoidal index grating, n_1 , is much less than the average index of the VHS, n_0 .

13. Those input ray deviations which are orthogonal to the direction of Bragg deviations are attenuated by Equation (50).

14. All angular measurements are made in radians.

2.10. Conclusion.

This chapter presented a first order model of the physics of the Holographic Projector which can be used to evaluate different Holographic Projector configurations and pixel/voxel mapping strategies. The model has been qualified by an appropriate set of assumptions. Also, a simple algorithm was presented which can be used to generate a first-order mapping strategy based on configuration parameter values.

This model is not necessarily a robust mathematical representation of the Holographic Projector. It is intended only to provide a mechanism by which the basic theory of the Holographic Projector can be analyzed to yield a level of expectation of its actual capabilities, and to provide a method by which the fabrication of many trial and error Volume Holographic Screens can be avoided.

3. PROOF-OF-CONCEPT POINT DESIGN

Thus far all Holographic Projector developments have been kept as general as possible so that future research can share a common beginning (that is, the model of Chapter 2). The purpose of this chapter is to present the rationale behind the selection of a specific, experimental Holographic Projector architecture which, if successful, will demonstrate that this technology deserves further attention. Accordingly, the scope of this proof-of-concept (POC) architecture is limited to the minimum amount of resources required to make such a demonstration effective yet practical. Optimization of the Holographic Projector, exhaustive validation of the model and determination of the full Holographic Projector parameter space are therefore topics of future studies.

3.1 *Implications of the Holographic Projector Model.*

The primary purpose of employing the Holographic Projector model is to provide a pixel/voxel mapping strategy which maximizes the diffraction efficiency of each correct pixel/voxel combination while minimizing that of all other combinations. One way of maximizing this signal-to-noise characteristic is to minimize the angular deviation from the Bragg angle which yields a given diffraction efficiency.¹ From Equation (3), we rewrite the value for δ , in the absence of Δ , as

$$\delta = \frac{C_s \alpha \lambda_a}{\pi T n_o \sin(2\theta_b)} \quad (51)$$

Further, transforming C_s to a function of the Bragg and slant angles (see Figure 3), and arbitrarily setting α to π yields

$$\delta_{(\alpha=\pi)} = \frac{\lambda_a \sin(\phi - \theta_b)}{T n_o \sin(2\theta_b)} \quad (52)$$

The obvious conclusion which can be made from Equation (52) is that maximum thickness, maximum average index of refraction and minimum wavelength are all desirable when creating the VHS in order

¹ It is well documented that diffraction efficiency generally decreases with deviation from the Bragg angle and writing wavelength (in accordance with our assumptions). See Kogelnik, Figures 6 and 12.

to maximize its angular selectivity (or to minimize diffractive crosstalk). To analyze the influence of the function $\sin(\Theta_b - \phi)/\sin(2\Theta_b)$, we refer to Figure 9 where this function has been calculated for certain values of Bragg and slant angles. Note that only the absolute values of the function are shown due to the irrelevance of sign.

		BRAGG ANGLE (DEGREES)									
		0.0	10.0	20.0	30.0	40.0	50.0	60.0	70.0	80.0	90.0
SLANT ANGLE (DEGREES)	0.0	1.00	0.51	0.53	0.58	0.65	0.78	1.00	1.48	2.88	1.00
	10.0	----	0.00	0.27	0.39	0.51	0.65	0.88	1.35	2.75	---
	20.0	----	0.51	0.00	0.20	0.35	0.51	0.74	1.19	2.53	---
	30.0	----	1.00	0.27	0.00	0.18	0.35	0.58	1.00	2.24	---
	40.0	----	1.48	0.53	0.20	0.00	0.18	0.39	0.78	1.88	---
	50.0	----	1.88	0.78	0.39	0.18	0.00	0.20	0.53	1.48	---
	60.0	----	2.24	1.00	0.58	0.35	0.18	0.00	0.27	1.00	---
	70.0	----	2.53	1.19	0.74	0.51	0.35	0.20	0.00	0.51	---
	80.0	----	2.75	1.35	0.88	0.65	0.51	0.39	0.27	0.00	---
	90.0	----	2.88	1.48	1.00	0.78	0.65	0.58	0.53	0.51	1.00

Figure 9. Functional Values of $\sin(\Theta_b - \phi)/\sin(2\Theta_b)$.

It is important to clarify that this analysis only considers angular sensitivity for a given diffraction efficiency. Thus these conditions are not necessarily optimum for all parameters (e.g. diffraction efficiency itself). At this time however, we are more concerned with achieving a well defined voxel grid (due to high angular selectivity) than we are with the issue of the light loss associated with low diffraction efficiency.

We now explore the effect of wavelength variation in the light used to illuminate the completed Holographic Projector. In the absence of δ , Equation (3) is manipulated in the same fashion as with Equation (52) to yield

$$\Delta_{(\alpha=\pi)} = \frac{\lambda_a^2 \sin(\Theta_b - \phi)}{2Tn_o \sin^2(\Theta_b)} \quad (53)$$

The Bragg and slant angle dependence of this function is shown in Figure 10.

		BRAGG ANGLE (DEGREES)									
		0.0	10.0	20.0	30.0	40.0	50.0	60.0	70.0	80.0	90.0
SLANT ANGLE (DEGREES)	0.0	1.00	5.76	7.92	2.00	1.56	1.31	1.15	1.06	1.02	1.00
	10.0	----	0.00	1.48	1.37	1.21	1.10	1.02	0.98	0.97	0.98
	20.0	----	5.76	0.00	0.69	0.83	0.85	0.86	0.87	0.89	0.94
	30.0	----	11.3	1.48	0.00	0.42	0.58	0.67	0.73	0.79	0.87
	40.0	----	16.8	2.92	0.69	0.00	0.30	0.46	0.57	0.66	0.77
	50.0	----	21.3	4.27	1.37	0.42	0.00	0.23	0.39	0.52	0.64
	60.0	----	25.4	5.49	2.00	0.83	0.30	0.00	0.20	0.35	0.50
	70.0	----	28.7	6.55	2.57	1.21	0.58	0.23	0.00	0.18	0.34
	80.0	----	31.2	7.40	3.06	1.56	0.85	0.46	0.20	0.00	0.17
	90.0	----	32.7	8.03	3.46	1.85	1.10	0.67	0.39	0.18	0.00

Figure 10. Functional Values of $\sin(\Theta_b - \phi)/\sin^2(\Theta_b)$.

Now, the most desirable VHS is one with maximum angular selectivity but minimum wavelength selectivity so that changes in pixel colors will result in corresponding changes in voxel colors. Unfortunately, there are no common areas in the two previous figures which exhibit both characteristics (although some areas are better than others). We will therefore focus on the characteristic of maximum angular sensitivity for the POC design, leaving the problem of color image generation for future development.

It is apparent from the angular selectivity trend of Figure 9 that the optimum holographic projector configuration will involve a preponderance of 45 degree slant and Bragg angles. This leaves an arbitrary choice between a transmission or reflection type of VHS. We will therefore choose the reflection type simply because the candidate material for the VHS exhibits best performance in the reflection mode.

3.2 Implications of the Mapping Algorithm.

Section 2.7 describes an algorithm which yields a somewhat optimized mapping of voxels to pixels. It is obvious that even this first-order algorithm is highly computer intensive both in speed and memory requirements. This algorithm was coded in C and

is included in Appendix A. While the code has been documented somewhat, it generally mirrors the algorithm described in Section 2.7. Additionally, only the working modules of the code are given. Certain graphic output routines have been excluded for clarity and are available from the authors.

The first use of this code was in determining the influence of the number of VHS elements used to approximate the continuous surface of the VHS. The data from several runs of a given Holographic Projector configuration with different numbers of VHS elements were compared to determine this influence. Although each resultant data set was not identical, the changes were negligible enough to justify using 3 X 3 elements for the generation of the POC map. It must be noted that this is not a general conclusion, but at least sufficiently appropriate for the scope of the POC effort. For even with this VHS element limitation, the POC map generation is estimated to require over 32 hours of 80286 CPU time (with 80287) to complete.

The computation time needed to run the mapping algorithm is the primary reason for limiting the number of voxels for the POC to 125 (5 X 5 X 5). The second reason for doing so is to limit the amount of fabrication time during which an operator must position each pixel/voxel combination.

3.3 The Chosen Proof-of-Concept Architecture.

The previous discussions, as well as certain practical considerations, lead to the following summary of desired characteristics of the POC Holographic Projector.

1. The VHS is a reflection volume hologram.
2. The display volume is 4in x 4in x 4in.
3. Field of view should be maximized.
4. Bragg angles should be roughly 45 degrees.
5. Slant angles should be roughly 45 degrees.
6. The device should be as thin as possible.
7. The display voxel space should be close to the viewer.
8. The pixel device should be positionally adjustable.

Once again, this point design does not necessarily describe an optimized Holographic Projector. It is intended only as a baseline architecture to demonstrate the technology.

4. PROOF-OF-CONCEPT FABRICATION

This chapter describes the conversion of the proof-of-concept point design into a working device. The goal of this conversion is to produce a device capable of demonstrating the general concept of the holographic projector using a minimum amount of resources. While all the details associated with the fabrication of the test device are not included, sufficient information is provided to understand the process.

4.1. VHS Configuration and Material.

Because of its ease of use and ideal suitability to this effort, DuPont's OMNIDEX 352 holographic film was the choice for the VHS.¹ This material is fairly new (January, 1990) and was provided by DuPont only through a joint nondisclosure agreement.

OMNIDEX 352 is a photopolymer material which is delivered sandwiched between two mylar sheets. For a rigid VHS sample, one of the sheets is peeled off so that the holographic material can be laminated to a 8in x 10in standard-glass plate (such as those in standard picture frames). This process is then duplicated for the other side. The result is a rigid VHS with symmetry on either side of the holographic material. This symmetry is important if the formed reflection planes are to be accessed from a conjugately placed pixel display in order to produce a conjugate image. Since the plate glass and the holographic material have roughly the same index of refraction, it is **assumed** that the presence of the plate glass does not significantly affect the mapping algorithm enough to alter it.

4.2. Proof-of-Concept Configuration.

The following geometry illustrates the configuration of the pixel display, VHS and voxel space for the POC. The values shown were those inserted into the mapping algorithm code to determine appropriate pixel/voxel combinations. This geometry incorporates the characteristics listed in Section 3.3. The pixel separation was determined as nine times the distance between two green pixels on the color TV. A central 70 x 70 grid of display pixels was used with only every 10th pixel considered a viable candidate - yielding

¹. OMNIDEX and DuPont are registered trademarks of E. I du Pont de Nemours & Company, Inc. Information about the OMNIDEX material is contained in two papers from the 1990 SPIE OE/Lase Conference Proceedings titled **Practical Holography IV**. The papers, written by the people at DuPont who developed the materials, are titled "Photopolymers for Holography" and "Hologram Recording in DuPont's New Photopolymer Materials".

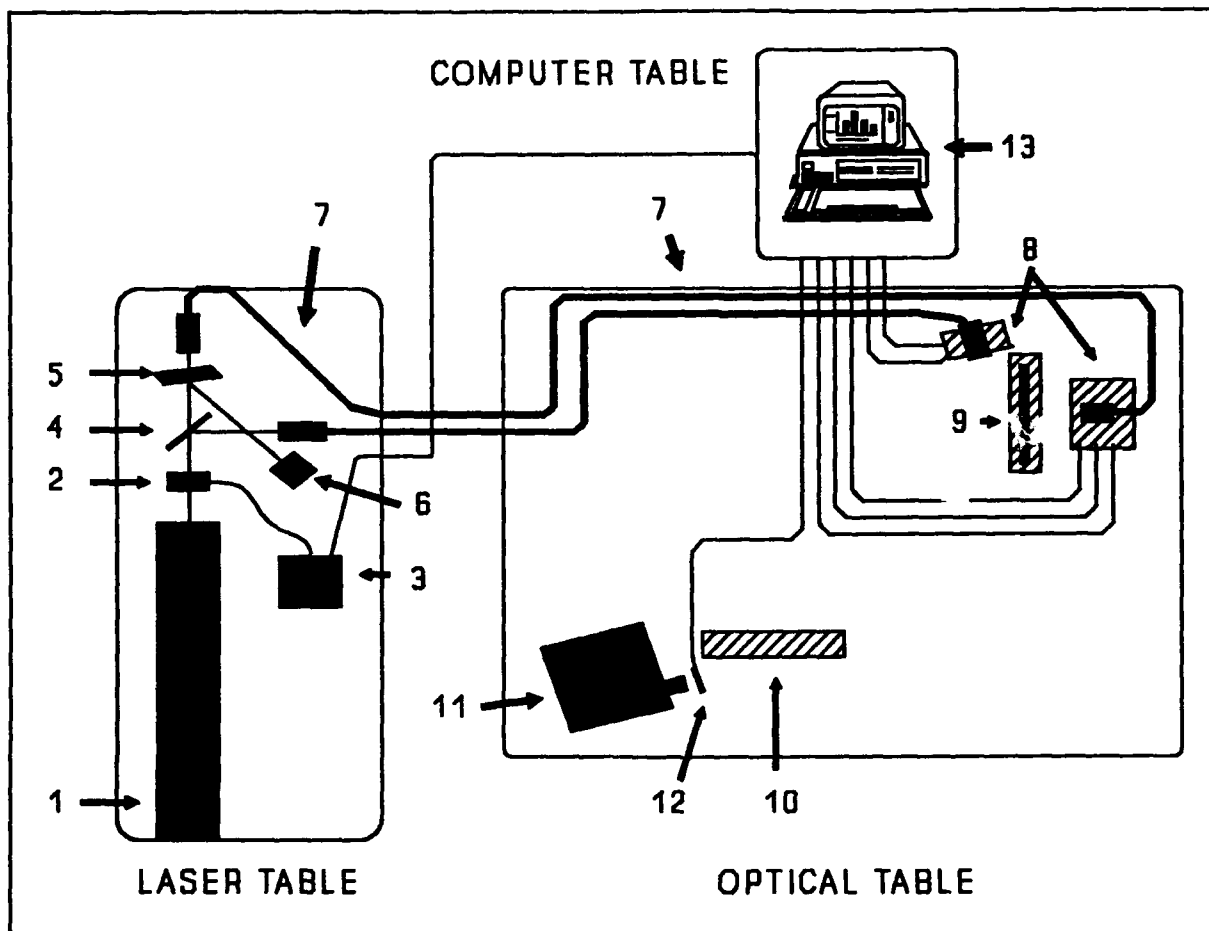


Figure 11. Proof-of-Concept Configuration.

a 7 x 7 grid of pixels.

4.3. Fabrication Equipment Setup.

Other than an oven and a ultraviolet curing lamp used to process the OMNIDEX material, all equipment used to fabricate (and demonstrate) the POC projector was placed on a vibration-isolated optical table and two nearby work tables (the "laser table" and the "computer table"). The setup is shown in Figure 12.

The following descriptions generally follow the path of laser light to the holographic setup. Also shown and described are the devices and layout for demonstrating the POC projector.

1. The laser system is 6.0 watt Argon ion laser outfitted and configured for single frequency operation of 2.4 watts at 514.5

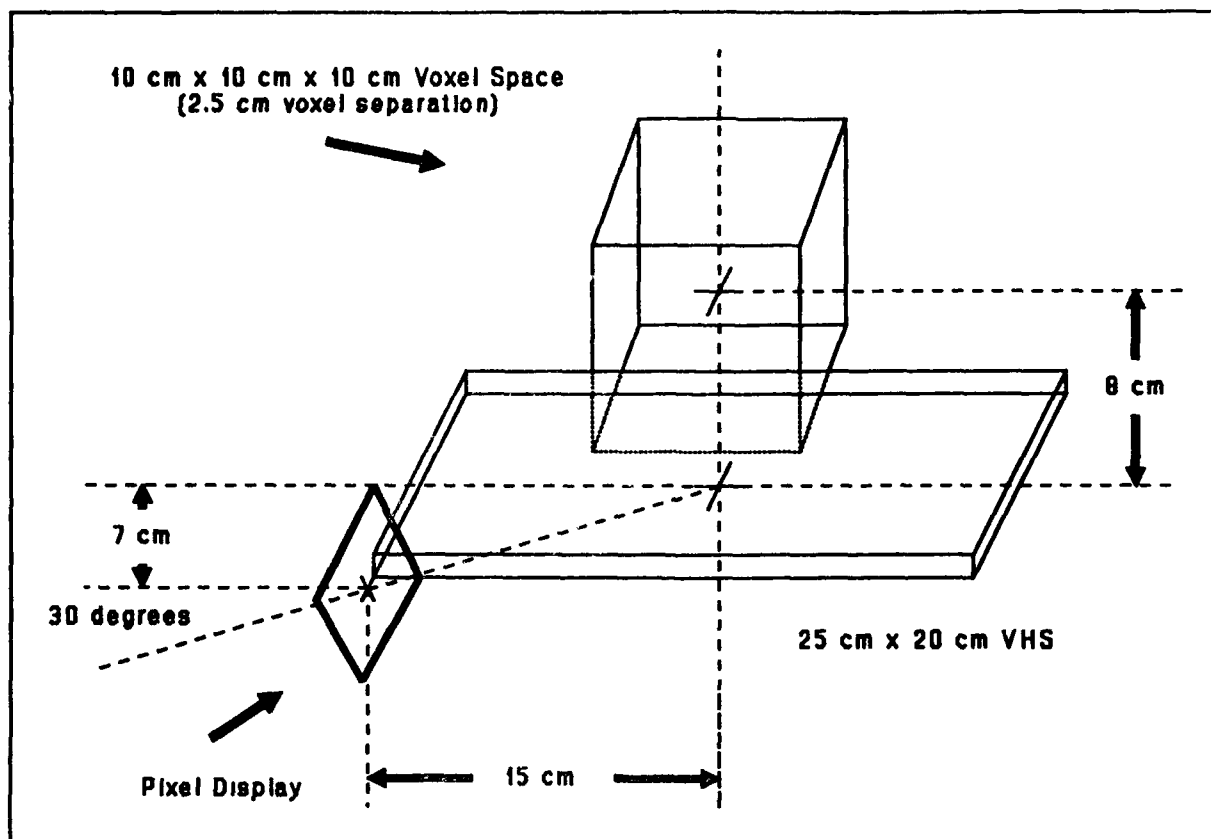


Figure 12. Proof-of-Concept Fabrication Setup.

nanometers.

2. The laser output first passes through a remotely controlled shutter.

3. The shutter remote controller also includes an electronic relay so that the beam can be controlled from a computer.

4. The beam is split into two beams with a conventional beam splitter.

5. A variable attenuator provides a capability of changing the relative strength of the two beams as well as providing beam sampling access for a spectrum analyzer.

6. A spectrum analyzer receives a sample of the beam and outputs to an oscilloscope so that the single frequency characteristic of the laser output can be monitored.

7. The two beams are directed into multimode fiber optic

cables which are bridged between the laser table and the optical table using rubber-bands to suppress vibration transfer. The ends of the cables have couplers which collimate the light into spatial filters consisting of 60x objectives and 5 micron pinholes.

8. The point source assemblies are mounted on motorized translation stages. The pixel source assembly consists of two stages capable of placing the pixel in any position of the 7 x 7 plane array discussed in Section 4.2. Likewise, the voxel source assembly consists of three stages to place its source in any of the 125 possible voxel positions of the POC Holographic Projector.

9. The VHS is mounted in a large film plate holder, which in turn is mounted to a base fixed to the optical table.

10. The base from the writing stage (9) has been duplicated here so that the film plate holder can be remounted in exactly the same orientation as it had in the writing stage.

11. A slide projector with no slide is used as a light source for the pixel display.

12. A color, liquid crystal TV was used as the pixel display.

13. A computer was used to direct the fabrication process and to drive the TV for demonstration and testing purposes. Five outputs controlled the motorized translation stages. One controls the shutter, with the remaining output connected to the TV. The software for the fabrication cycle simply steps through each pixel/voxel combination given by the mapping algorithm output. With each step, the pixel and voxel sources are positioned and the shutter opened. All cables except for the shutter cable were bridged to the optical table using rubber-band suspension.

4.4. Fabrication Procedures.

The general procedures to be used for fabrication of the POC Holographic Projector are described below. A detailed description of the experiments actually performed is included in Chapter 5.

4.4.1. Generate the Pixel/Voxel Map.

The code in Appendix A was used to generate the pixel/voxel map for the POC. The input values in that code were those actually used. The resultant file was then made available to the software used by the controller computer used in the fabrication process.

4.4.2. Prepare the Hardware/Software.

This procedure involved warming-up the laser, insuring actuators were at nominal configurations and loading the fabrication program into the controller computer. Once loaded, this software then paused until told that all conditions were ready.

4.4.3. Load the Blank VHS.

A Volume Holographic Screen was made in accordance with Section 4.1 under red light. It was then mounted into a film plate holder. The holder was then secured to the writing stage base between the voxel and pixel point sources (ref. Fig. 12).

4.4.4. Expose the VHS.

The controller computer was then allowed to proceed through the pixel/voxel map to control the equipment and form the many holograms in the VHS.

4.4.5. Process the VHS.

The VHS, still in the plate holder, was flooded with ultraviolet light to fix the photoreactive nature of the OMNIDEX material. It was then heated to roughly 100 degrees celsius for one hour to maximize the diffraction efficiency of the material. These procedures were performed by recommendation from the articles cited in Footnote 5.

4.4.6. Integrate the VHS into the POC.

The plate holder and VHS was mounted to the base in the read stage. At this point, the Proof-of-Concept Holographic Projector was complete and ready for testing.

5. EXPERIMENTS AND RESULTS

The purpose of this chapter is to provide the results of experiments done in the XPK Laser/Optics Laboratory. A series of four experiments were planned, leading to the fabrication of the POC device. Experiment 1 involved testing the output of optical fibers. Experiment 2 tested angular selectivity of different film thicknesses. Experiment 3 was to validate the exposure requirements of the film, and experiment 4 investigated the angular selectivity of multiplexed holograms.

5.1 Experiment 1

The output of the multimode optical fibers used to transfer laser light onto the optical bench was tested for coherence with a Michelson interferometer. Tests were conducted both with and without spatial filtering (the filter consisted of a 60X microscope objective and a 5 micron pinhole). No interference fringes could be found in either case, leading to the conclusion that coherence was lost in propagation through the fibers. To eliminate this problem the fibers were removed and the Argon ion laser, the shutter, and the beam splitter were moved onto the optical bench (Figure 12). Beams were directed around the table with a series of mirrors mounted on motorized translation stages. The point sources required for recording pixels and voxels were provided by expanding the beam through 40X microscope objectives. Vibrations in the optical bench created by the cooling water flow through the laser were isolated using a pair of bicycle innertubes supported by a hardwood frame. With the new equipment setup a coherence length of at least 2m was established, again using the Michelson interferometer.

5.2. Experiment 2

The next experiment tested the angular selectivity of holograms recorded in Dupont Omnidex 352 Holographic Recording Film. In order to test various film thicknesses, layers of the photopolymer were laminated on top of each other. The film was 25 microns thick and the number of layers varied from 1 to 16 giving a range of film thickness from 25 to 400 microns. Each layer was separated from the next by a thin mylar sheet. A recording was made of a single pixel - voxel pair in each of the 3.5in x 4.5in film samples. Qualitative inspection showed that:

1. A narrow band source is necessary for good angular selectivity,
2. Hologram brightness increased with the number of film layers,
3. Angular selectivity generally decreased with the number of film layers,

4. The diffraction efficiency vs. deviation from the bragg angle exhibited the center maximum and decreasing side lobes predicted by theory.

The decrease in angular selectivity with increasing numbers of film layers is most probably due to reflections off the various mylar - film interfaces. All further experiments were accomplished with single layers of film to get maximum angular selectivity.

5.3. Experiment 3

A qualitative test of exposure vs. image quality was done to verify Dupont's data and to gain experience working with the material. The test consisted of recording single pixel - voxel pairs in 3.5in x 4.5in film samples at a range of exposure levels. The pixel and voxel were each the center point of their respective spaces shown in Figure 11. Due to the recording geometry and the uneven illumination of the film from the point sources, it was impossible to determine actual exposure levels over the entire film surface. However, with 0.35 watt of power out of the Argon ion laser (mainly 51'.5 nm), exposure times ranging from 30 sec to 240 sec, and the recording geometry shown in Figures 11 and 12, it was found that a 90-sec exposure gave the brightest and sharpest image. This corresponds approximately to the Dupont exposure requirement of 30 mJ/cm².

5.4. Experiment 4

Five pixel-voxel pairs were recorded in a single 7.5in x 8.5in sheet of photopolymer to test the selectivity of an angularly multiplexed hologram. The voxels were along the lower right hand edge of the voxel space shown in Figure 11, the corresponding pixels were determined by the mapping routine described in Section 2.7. Crosstalk between the pixels was much greater than that predicted by Collier's "rule of thumb" (Equation 52). This prompted the computer analysis which is summarized in Chapter 6.

6. ANALYSIS AND CONCLUSIONS

The purpose of this chapter is to first, analyze the results of experiments done in the AAA-2 Laser/Optics Laboratory, and second, give conclusions on the entire research effort discussed in this paper.

6.1. Analysis

The experiments in Chapter 5 led to the conclusion that crosstalk was a much greater problem than had been anticipated in the original analysis. Accordingly, the diffraction efficiency equations (Equations (1) and (2)) for both transmission and reflection holograms were reexamined using a computer simulation (Appendix A). The diffraction efficiencies have been plotted against read/write beam deviation for a number of thicknesses in Figures 13 and 14. The pixel and voxel used as the recording pair in the simulation were located at the center of their respective spaces as shown in Figure 11. The recording medium was taken to be Dupont Omnidex 352 HRF ($n_0 = 1.5$, $n_1 = 0.03$), exposed with 514.5nm light from an Argon ion laser.

From these figures it is apparent that Equation 52, which claims that angular selectivity increases with increasing film thickness, does not hold for very thick holograms. With a reflection hologram, if the index of refraction modulation (n_1) is held constant while the thickness of the film is increased, angular selectivity reaches a lower limit. In this case, the number of addressing pixels is severely restricted since the limit is around 2.5 degrees for practical Volume Holographic Projector geometries. For a transmission hologram, large side lobes in the diffraction efficiency function prevent a high addressing pixel density. A very thick transmission hologram does not exhibit angular selectivity in the conventional sense and cannot be used for this display. For reflection holograms, matching the first zero of one pixel with the edge of the central lobe of the next gives the minimum possible pixel spacing. This corresponds to an angle of roughly 4 degrees for the Volume Holographic Projector geometry. Even at this spacing there will be a large amount of crosstalk between the pixels. As a more conservative approach, at 10 degrees spacing the side lobes have fallen to roughly 10 percent of the peak value so that crosstalk will be much lower. However, such a spacing represents so few available 3-D pixel sites that the device would be impractical for pixel-based imaging.

6.2. Conclusions

The Volume Holographic Projector was intended to make real-time computer generated holography a reality by reducing both data

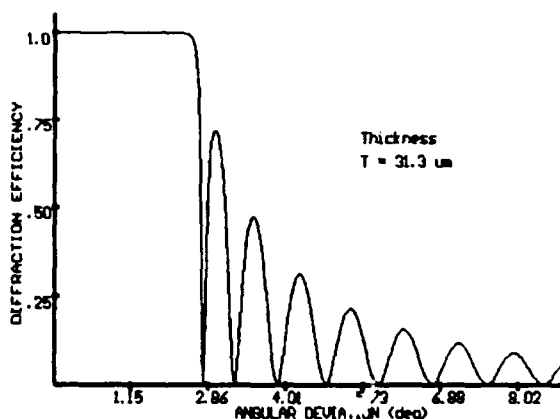
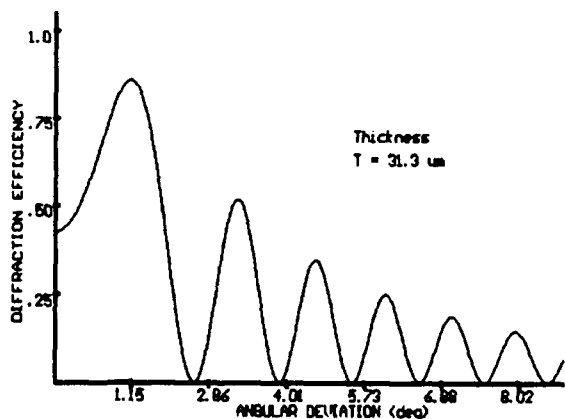
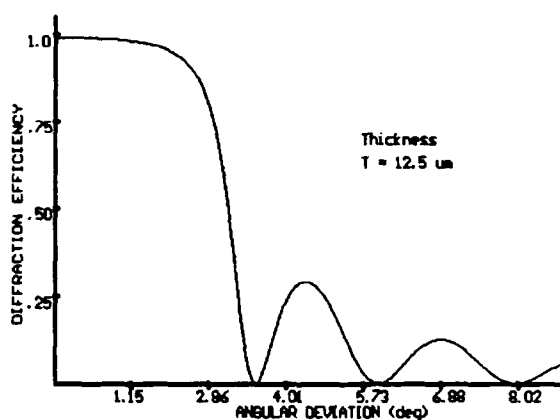
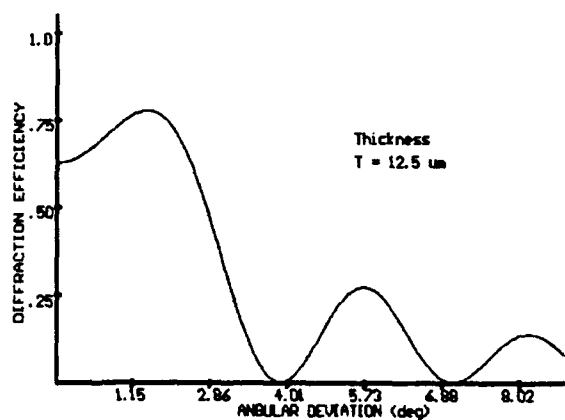
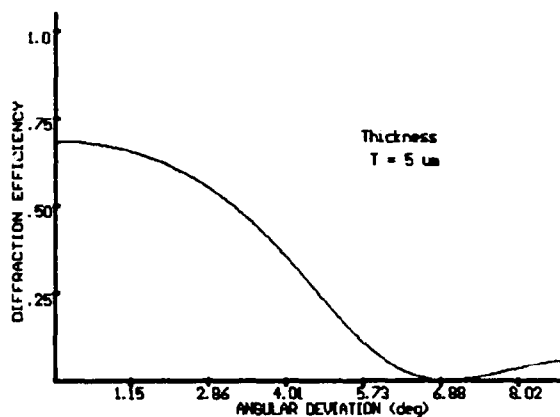
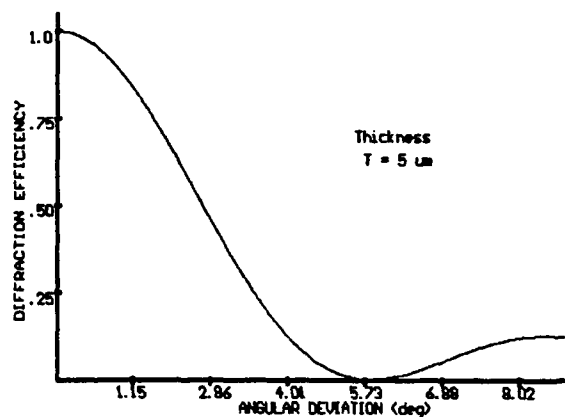


Figure 13. Diffraction Efficiency vs. Read/Write Beam Angular Deviation for Transmission Holograms.

Figure 14. Diffraction Efficiency vs. Read/Write Beam Angular Deviation for Reflection Holograms.

bandwidth and the amount of calculation required to display holograms. These two objectives were to be met by recording a series of independently addressable holograms within a volume

holographic recording medium, then playing them back individually using the pixels from a spatial light modulator as reference beams. Data bandwidth is thus reduced since only the reference signal corresponding to a wavefront needs to be transmitted to the display, not the entire wavefront. Computation time is also reduced since the interference pattern which forms the hologram is stored in the film and does not need to be calculated. Unfortunately, crosstalk between the separate holograms prevents the development of a pixel based device such as the Volume Holographic Projector.

The main conclusion of this study is that the storage capabilities of volume holograms are severely limited when a strict one-to-one mapping of input to output is required. Such a mapping limitation does not allow for the creation of high density pixel based images. However, since the projected images are not restricted to point sources, there may be some uses for which this device is suited (i.e., threat warning or attitude/directional indicators). Future work in this laboratory will determine both what those uses are and how practical a display of this type would be in the cockpit.

REFERENCES

1. Veron, H., D. Southard, J. Leger, and J. Conway, "3D Displays for Battle Management," The MITRE Corporation, Bedford, MA, 01730, published as RADC-TR-90-46 (April 1990).
2. Wilson, A., "At SID, Lasers Put New Spin on 3D Displays," ESD: The Electronic System Design Magazine, August 1988, pp. 17-18.
3. Lim, T., "A Varifocal Fresnel Lens for Stereoscopic Display," Amerasia Technology Inc., 630-1 Hampshire Road, Westlake Village, CA, 91361, published as RADC-TR-89-148 (June 1989).
4. St. Hilaire, P., S. Benton, M. Lucente, M. Jepsen, J. Kollin, H. Yoshikawa, and J. Underkoffler, "Electronic Display System for Computational Holography," SPIE, Vol 1212, pp. 325-333, (January 1990).
5. Meacham, G., "Autostereoscopic Displays - Past and Future," SPIE, Vol 624, pp. 90-101 (January 1986).
6. Kogelnik, H., "Coupled Wave Theory for Thick Hologram Gratings," Bell System Tech J., 48, 2909 (November 1969).
7. Collier, R., C. Burckhardt, and L. Lin, Optical Holography, Academic Press, New York, 1971.
8. Weber, A., W. Smothers, T. Trout, and D. Mickish, "Hologram Recording in DuPont's New Photopolymer Materials," SPIE Vol 1212, pp. 20-29 (1990).
9. Klein, W., "Theoretical Efficiency of Bragg Devices," Proc. IEEE, 54, 803 (1966).

APPENDIX A

Mapping Algorithm Computer Code

```

#include <graphics.h>
#include <math.h>
#include <stdio.h>
#include <conio.h>
#include <vgdsuprt.h> /* support code with declarations and graphics */

void INPUT_FUNCTION()
{
    na      = 1.004;
    no      = 1.5;
    Pix_dim = 6; /* These values are N of 2N+1 units per edge */
    Vox_dim = 2;
    VHS_dim = 2;
    VHS_side = 200.0; /* All distances are in millimeters */
    Vx      = 0.0;
    Vy      = 0.0;
    Vz      = -114.0;
    Px      = -170.0;
    Py      = 0.0;
    Pz      = 80.0;
    Lambda_a = 0.0005145;
    Read_W   = 0.0005145;
    T        = 0.025;
    pix_inc  = 4;
    vox_inc  = 25;
    VHS_inc  = VHS_side/(2*VHS_dim);
    Theta_V  = 0.0; /* radians */
    Theta_P  = 1.0472;
    Total_index_variation = 0.1;
}

/*****
/*
/*                               PIXEL/VOXEL MAPPING MODULE
/*
/*      This module determines the mapping of each voxel to a pixel in
/*      accordance with the algorithm provided in chapter two. The results are
/*      contained in the file VGDMAP. This module makes use of the Function
/*      DE to make the code more easily readable. Also produced is the
/*      variable QPV, which characterizes the aggregate signal to noise for
/*      the chosen configuration.
/*
*****/

void MAPROUTINE()
{
    int    A, B, C, F, G, Last_F, Last_G, locvox, locpix, Last_F_start,
           Last_G_start;
    int    Pix_dim1, FpPix_dim1, GpPix_dim1;
    float  a1,a2;
    float  TSN, TestSN, a, b, c;
    float  MS, denom;
    int    M, N, F_sub, G_sub;
    float  m,n,f,g,h,fq,gq,hq;

    QPV = 0.0;
    PIXFILLEDMAP[0][0] = 0;

```

```

locvox=0;
Last_F_start = -Pix_dim-1;
Last_G_start = -Pix_dim-1;
Pix_dimp1 = Pix_dim + 1;
for (A=-Vox_dim;A<=Vox_dim;A++)
{
    a1 = Vx + A*volinccsth;
    a2 = Vz + A*volincsnth;
    for (B=-Vox_dim;B<=Vox_dim;B++)
    {
        b = Vy + B*vox_inc;
        for (C=-Vox_dim;C<=Vox_dim;C++)
        {
            locvox++;
            locpix=0;
            a = a1 + C*volincsnth;
            c = a2 + C*volinccsth;
            TSN = 0.0;
            Last_F = Last_F_start;
            Last_G = Last_G_start;
            for (F=-Pix_dim;F<=Pix_dim;F++)
            {
                fq = Px + F*pixinccsth;
                hq = Pz + F*pixincsnth;
                FpPix_dimp1 = F + Pix_dimp1;
                for (G=-Pix_dim;G<=Pix_dim;G++)
                {
                    locpix++;
                    GpPix_dimp1 = G + Pix_dimp1;
                    if (PIXFILLEDMAP[FpPix_dimp1][GpPix_dimp1]==0)
                    {
                        MS=0;denom=0;
                        gq = Py + G*pix_inc;
                        for (M=-VHS_dim;M<=VHS_dim;M++)
                        {
                            m = M*VHS_inc;
                            for (N=-VHS_dim;N<=VHS_dim;N++)
                            {
                                n = N*VHS_inc;
                                MS = MS + DE(a,b,c,m,n,fq,gq,hq,fq,gq,hq,0);
                            }
                        }
                    }
                    for (F_sub=-Pix_dim;F_sub<=Pix_dim;F_sub++)
                    {
                        f = Px + F_sub*pixinccsth;
                        for (G_sub=-Pix_dim;G_sub<=Pix_dim;G_sub++)
                        {
                            g = Py + G_sub*pix_inc;
                            h = Pz + F_sub*pixincsnth;
                            if ((F_sub!=F) && (G_sub!=G))
                            {
                                for (M=-VHS_dim;M<=VHS_dim;M++)
                                {
                                    m = M*VHS_inc;
                                    for (N=-VHS_dim;N<=VHS_dim;N++)
                                    {
                                        n = N*VHS_inc;
                                        denom = denom + DE(a,b,c,m,n,f,g,h,fq,gq,hq,1);
                                    }
                                }
                            }
                        }
                    }
                }
            }
        }
    }
}

```

```

    }
    if (denom>0) TestSN = MS/denom;
    else {if (MS>0) TestSN = 1.0e+10;else TestSN=0;}
    if (TestSN>TSN)
    {
        PIXFILLEDMAP[Last_F+Pix_dimp1][Last_G+Pix_dimp1] = 0;
        Last_F = F;
        Last_G = G;
        PIXFILLEDMAP[FpPix_dimp1][GpPix_dimp1] = 1;
        TSN = TestSN;
    }
    Showpixpos(locpix);
}
}
fprintf(vgdmap,"%d %d ",Last_F,Last_G);
QPV=QPV+TSN;
Showvoxpos(locvox,QPV);
}
}
}

/*****
/*                      END OF PIXEL/VOXEL MAPPING MODULE                      */
*****/

/*****
/*                      DIFFRACTION EFFICIENCY FUNCTION                      */
/*
/*      This function computes the PLANE WAVE diffraction efficiency for a
/*      a given pixel/voxel/VHS location configuration.  The input variables are
/*      the physical locations of these points - not indices.  The procedures for
/*      computing the vector p and the attenuation factor Q are only necessary
/*      when the pixel examined is different than the pixel used to form the
/*      hologram.
/*
*****/

float      DE(float de_a, float de_b, float de_c,
              float de_m, float de_n,
              float de_f, float de_g, float de_h,
              float de_fq, float de_gq, float de_hq,
              int QON)
{
    float DE_value;
    float valtst, perterm;
    double mMa, nMb, mMfq, nMgq, mMf, nMg, mMa2pnMb2, mMfq2pnMgq2,
           mMf2pnMg2;
    double rz, sz, pz, rmag, smag, pmag;
    double ri, rj, rk, si, sj, sk;
    double ipi, ipj, ipk, ipmag, jpi, jpj, jpk, jpmag, kpi, kpj, kpk;
    double argmnt, Theta, Theta_b, Delta;
    float betatemp, Beta2, alphatemp, Alpha2, qtmp, Q, AlphaBetaterm, A2oB2;

    mMa = de_m - de_a;
    nMb = de_n - de_b;
    mMfq = de_m - de_fq;
    nMgq = de_n - de_gq;
    mMf = de_m - de_f;
    nMg = de_n - de_g;

```



```

mMa2pnMb2 = (mMa*mMa + nMb*nMb);
mMfq2pnMgq2 = (mMfq*mMfq + nMgq*nMgq);
mMf2pnMg2 = (mMf*mMf + nMg*nMg);

```

```

/* Calculation of equations 32, 33 and 34 */
/* signed for reflection hologram */

```

```

rz = -Indxratio*sqrt(de_c*de_c + mMa2pnMb2*Indxfactor);
sz = Indxratio*sqrt(de_hq*de_hq + mMfq2pnMgq2*Indxfactor);
pz = Indxratio*sqrt(de_h*de_h + mMf2pnMg2*Indxfactor);
rmag = sqrt(mMa2pnMb2 + rz*rz);
smag = sqrt(mMfq2pnMgq2 + sz*sz);
pmag = sqrt(mMf2pnMg2 + pz*pz);

```

```

/* Calculation of equations 35, 36 and 37 */

```

```

ri = mMa/rmag;
rj = nMb/rmag;
rk = rz/rmag;
si = mMfq/smag;
sj = nMgq/smag;
sk = sz/smag;

```

```

/* Calculation of equation 38 */

```

```

ipi = sj*rk - sk*rj;
ipj = sk*ri - si*rk;
ipk = si*rj - sj*ri;
ipmag = sqrt(ipi*ipi + ipj*ipj + ipk*ipk);
ipi = ipi/ipmag;
ipj = ipj/ipmag;
ipk = ipk/ipmag;

```

```

/* Calculation of equation 39 */

```

```

jpi = ri + si;
jpj = rj + sj;
jpk = rk + sk;
jpmag = sqrt(jpi*jpi + jpj*jpj + jpk*jpk);
jpi = -jpi/jpmag;
jpj = -jpj/jpmag;
jpk = -jpk/jpmag;

```

```

/* Calculation of equation 40 */

```

```

kpi = ipj*jpk - ipk*jpj;
kpj = ipk*jpi - ipi*jpk;
kpk = ipi*jpj - ipj*jpi;

```

```

/* Calculation of equation 41 */

```

```

argmnt = mMf*kpi + nMg*kpj + pz*kpk;
Theta = acos(-argmnt/pmag);

```

```

/* Calculation of equation 42 */

```

```

argmnt = ri*jpi + rj*jpj + rk*jpk;
Theta_b = acos(-argmnt);

```

```

/* Calculation of equation 44 */

```

```

betatemp = cl*(rj*sj + rk*sk);
Beta2 = -betatemp*betatemp/(rk*sk);

```

```

/* Calculation of equation 45 */

```

```

alphatemp = (Theta-Theta_b)*c2*sin(2*Theta_b)/sk;
Alpha2 = alphatemp*alphatemp;

```

```

/* Calculation of Diffraction Efficiency */

```

```

/* for a reflection hologram */
AlphaBetaterm = Beta2 - Alpha2;
if (AlphaBetaterm >= 0)
{
    perterm = 1/tanh(sqrt(AlphaBetaterm));
    perterm *= perterm;
}
else
{
    perterm = 1/tan(sqrt(-AlphaBetaterm));
    perterm = -perterm*perterm;
}
A2oB2 = Alpha2/Beta2;
DE_value = 1/(A2oB2 + (1-A2oB2)*perterm);

/* Calculation of Q if needed (equation 50) */
if (QON)
{
    if (jpk!=0) qtmp = (mMf*ipi + nMg*ipj + pz*ipk)/(mMf*jpi + nMg*jpj +
        pz*jpk);
    else qtmp=0;
    Q = 1/(1 + qtmp*qtmp);
    DE_value = DE_value*Q;
}
return(DE_value);
}

/*****
*/
END OF DIFFRACTION EFFICIENCY FUNCTION
*/
/*****/

void main()
{
    INPUT_FUNCTION();
    INITIAL();
    WORK_DISPLAY();
    CHECK_INPUT();
    if (Check==0)
    {
        setcolor(11);
        outtextxy(350,290,"Enter any key to begin ...");
        getch();
        setfillstyle(1,0);
        bar(349,280,615,310);
        setcolor(11);
        outtextxy(350,290,"Working ...");
        setfillstyle(1,LIGHTRED);
        vgdmap = fopen("d:pocmap.dat","w"); /* file on ramdisk */
        fprintf(vgdmap,"%d %d %d %d %d ",(int)
            (Lambda_a*10000000),Vox_dim,VHS_dim,Pix_dim,(int) (T*1000));
        MAPROUTINE();
        fclose(vgdmap);
        setfillstyle(1,0);
        bar(349,290,615,310);
        setcolor(11);
        sound(350);delay(25);nosound();
        outtextxy(350,290,"Mapping complete.");
        outtextxy(350,310,"Enter any key to exit ...");
        getch();
    }
    closegraph();
}

```

APPENDIX B

Plans and Procedures

LASER SYSTEM SETUP

- * set up power meter
- * set up heat exchanger and water cooler (follow manual)
 - * fill
 - * set temperature
 - * run
 - * check for leaks
- * set up laser (follow manual)
 - * write start-up procedure
 - * fire laser and align diagnostic equipment
 - * experiment with system
 - * set up spectrum analyzer and oscilloscope
 - * install etalon
 - * optimize laser
 - * record and store conditions
- * safety certification

FIBER OUTPUT TEST PLAN

- * configure input table
- * set up power meter
- * align input
- * align output
- * align interferometer
- * check polarization
- * check coherence
- * check stability

POC CONFIGURATION PLAN

- * install actuators and boards
- * position point sources
- * position power meter
- * maximize output power and polarization
- * determine exposure
- * determine VHS configuration
- * finalize automation
- * practice with holographic materials
- * write fabrication procedures

VHS FABRICATION PROCEDURES

1. Prepare VHS blank in bracket. Place in light-proof container.
2. Remove extraneous equipment and materials.
3. Turn on computer. Load fabrication program.
4. Initialize actuators at nominal positions.
5. Follow laser start-up procedures.
6. Ensure laser is operating normally.
7. Verify power levels.
8. Configure shutter controller for correct exposure time.
9. Float the optical bench.
10. Turn off the lights.
11. Mount VHS blank on bench.
12. Run fabrication program.
13. Turn laser off (Don't shut down).
14. Remove VHS and flood with UV light.
15. Place VHS in oven for 60 minutes at 200 °F.
16. Follow laser shut down procedures.